TÜBİTAK

Turkish Journal of Chemistry

http://journals.tubitak.gov.tr/chem/

Research Article

Turk J Chem
(2018) 42: 1056 – 1071
© TÜBİTAK
doi:10.3906/kim-1712-47

Development of a nanoscale-based optical chemical sensor for the detection of NO radical

Özlem ÖTER[1,*], Akif Cihan AYDIN[2], Merve ZEYREK ONGUN[3], Erdal ÇELİK[4]

[1]Department of Chemistry, Faculty of Science, Dokuz Eylül University, İzmir, Turkey
[2]Graduate School of Natural and Applied Sciences, Dokuz Eylül University, İzmir, Turkey
[3]Technical Programs Department, İzmir Higher Vocational School, Dokuz Eylül University, İzmir, Turkey
[4]Center for Fabrication and Application of Electronic Materials (EMUM), Dokuz Eylül University, İzmir, Turkey

Received: 21.12.2017 • **Accepted/Published Online:** 02.04.2018 • **Final Version:** 03.08.2018

Abstract: Nitric oxide is one of the most important biochemical parameters in biological processes; it is also known as carcinogenic. There is need for the design of stable and durable solid phase nitric oxide sensors. In this study, we immobilized the nitric oxide sensitive molecules pyrene, tris(2,2'-bipyrdyl)dichlororuthenium(II) hexahydrate ($Ru(bipy)_3^{2+}$), and magnesium phthalocyanine (Mg-Pc) for the first time in polymeric or glassy matrices. We applied silver nanoparticles and ionic liquids in the fabrication process of polymeric electrospun fibers and thin films. We compared their NO sensitivity in micelle solutions that mimic the cell medium by both steady state and lifetime-based fluorescence measurements. Among the tested dyes, the pyrene exhibited the highest response for radicalic NO. The Mg-Pc dye followed pyrene in terms of sensitivity and exhibited increasing fluorescence intensity and lifetime-based response. Lifetime-based response is advantageous and selective as it is not affected by source variations, photo-bleaching, or leaching effects. Another advantage of Mg-Pc dye is that it is not poisonous for organic systems. Presence of the ionic liquid enhanced the sensor response in all of the test moieties. The obtained limit of detection values for pyrene, $Ru(bipy)_3^{2+}$ and Mg-Pc dyes were 0.15 μM, 1.54 μM, and 0.78 μM, respectively.

Key words: Nitric oxide radical, time resolved fluorescence, nanomaterials, electrospinning, pyrene, ruthenium complex, magnesium phthalocyanine

1. Introduction

Nitric oxide is the smallest reactive oxygen species and the key biochemical messenger and biological signaling molecule in cells. It also has an important role in immune and blood pressure regulation systems.[1−3] Therefore, real-time sensor development studies for nitric oxide attract great attention for biomedical research and diagnosis. Many analytical techniques have been used for detection of NO relying on electrochemistry,[4−6] chromatography,[7,8] electron paramagnetic resonance spectroscopy (EPR),[9,10] and optical chemical sensors.[11−24] From these, optical chemical sensors are good alternatives because of their high sensitivity, low cost, relative simplicity, and real-time detection ability.[11,12,15,16,18] Many fluorescence-based sensors for NO detection have been reported to date.[11−21] A short summary of these sensors for nitric oxide in terms of sensing agents, matrix materials, working ranges, and detection limits is given in Table 1. Most of these studies are sensors in solution phase.[12−14,17,19,21] Some are solid phase sensors based on entrapment of the sensing dye in different

*Correspondence: ozlem.oter@deu.edu.tr

matrix materials such as nafion, mesoporous silica, cellulose acetate, polycaprolactone, and poly 2-hydroxyethyl methacrylate.[11,15,16,18] The suggested sensor uses the solid PVC and sol gel matrix material, which plays an important role in the stability and sensitivity of the sensor. The analyte-permeability of the solid matrix directly influences the sensitivity. On the other hand, the host/dye compatibility is another important issue and poor compatibility may result in leaching or dye aggregate formation on either the micro- or nanoscale. Depending on the selected polymer, the indicator dyes possess moderate to high photostabilities. However, there is a need for the development of stable solid phase sensors. Polyvinyl chloride (PVC) and sol-gel possess excellent compatibility with the indicator dyes, resistant characteristics to water and harsh conditions, protecting abilities of the indicator dyes from alterations providing an appropriate microenvironment for them, and tailoring abilities (for PVC) in electrospinning conditions. The sensing agents utilized in the reported studies are mostly focused on fluorescent metal complexes of diaminofluorescein, diaminonaphthalene, and diaminoanthraquinone derivatives.[11−21] They use steady state measurements based on the emission intensity enhancement of the dyes that directly react with NO. In this study, the indicators utilized were fluorescent dyes of pyrene, magnesium phthalocyanine (Mg-Pc), and tris(2,2'-bipyrdyl)dichlororuthenium(II) ($Ru(bipy)_3^{2+}$) hexahydrate, which were tested for the first time for the detection of NO in solid matrices. These dyes were chosen because they are moderately cheap, easily available commercial dyes that are well known with their sensing capability for gaseous oxygen and reactive oxygen species. Moreover, all of the utilized dyes have long fluorescence lifetimes so that both steady state and lifetime-based measurements can be employed. Lifetime-based response is advantageous and selective as it is not affected by source variations, photo-bleaching, or leaching effects. The sensing dyes were entrapped in both thin film and electrospun membranes in the presence and absence of different additives such as nanosized silver and ionic liquids, which are known as effective on the fluorescence characteristics of the sensing agents and facilitate the detection capability of the sensing probe.[25] Thus, these additives were utilized for the first time for nitric oxide sensing purposes and a significant enhancement of sensor response was obtained. The obtained limit of detection values of 10^{-7} mol L^{-1} are less than most of the LOD levels given in the literature for solid phase optical sensors.[15,11,18,20] Furthermore, the suggested sensor has a wide dynamic working range from 10^{-7} to 10^{-4} mol L^{-1} levels

2. Results and discussion

2.1. Surface structure of the sensing materials

In this work, we employed ionic liquids and AgNPs in PVC membranes in either thin film forms or microfiber structures. Thus, we compared the sensing capability of thin films with fiber structures. Figures 1a and 1b and 1c and 1d are the SEM images of the pyrene containing electrospun mats in the absence and presence of AgNPs, respectively. Figures 2a and 2b and 2c and 2d are the SEM images of the Mg-Pc doped slides in the absence and presence of AgNPs, respectively. The electrospun membranes of both dyes exhibited good adhesion to the aluminum substrate. It was observed that the membrane had a 3-dimensional network with a porous structure. These pores within the network structures allow the diffusion of small nitric oxide molecules. In Figures 1c and 1d and Figures 2c and 2d, the presence of silver nanoparticles can be seen as gray clusters on the surface. The presence of AgNPs caused a slight increase in the porosity of the membranes. From the figures, we observe thinner fiber structures and smaller but increasing amounts of holes in the presence of AgNPs. Moreover, AgNPs increased the electrical conductivity and facilitated the electrospinning process. These results are in agreement with the literature results. Wang et al. found that the use of silver nanoparticles in electrospinning resulted in highly porous nanofibrous membranes.[26] In addition, it is known that the presence of ionic liquids enhances the

Table 1. A short summary of the nitric oxide sensing studies .

Sensitive dye	Matrix material and/or media	Dynamic working range	Detection limit	Ref.
Bis[(2,9-dimethyl-1,10-phenanthroline)] copper (II) complex	Nafion	0–2.5 μmol L^{-1}	0.32 μmol L^{-1}	15
$Rh_2(AcO^-)_4$(Ds-pip), $Rh_2(AcO^-)_4$ = Rhodium(II) acetate, Ds-pip = dansyl-piperazine	Microbead/mesoporous silica	Not reported	Not reported	11
Diaminofuorescein DAF-FM and its diacetate	Rat bladder smooth muscle cells	2–200 nmol L^{-1}	3 nmol L^{-1}	12
Copper(II) complex CuQNE with a naphthalimide-containing ligand	Aqueous solution	Not reported	1 nM in aqueous solution	13
N^1,N^1-dimethylethane- 1,2-diamine, N^1,N^1-dimethyl-N^2-{(pyridin-2-yl)methyl}ethane-1,2-diamine	Water, methanol and acetonitrile media	Not reported	~10 nmol L^{-1}	14
CdSe quantum dots (QDs)	Cellulose acetate	1.0×10^{-7} to 1.0×10^{-6} mol L^{-1}	1.0×10^{-8} mol L^{-1}	16
DAN/β-CD, DAN=2,3-diaminonaphthalene, β-CD = β -cyclodextrin	Phosphate buffer	0–5 μM	~20 nmol L^{-1}	17
Copper(II)naphthalene-sulfonamino-quinoline	Polycaprolactone	0–2.4 mmol L^{-1}	12 ± 0.2 μmol L^{-1}	18
8-(3',4'-diaminophenyl)-difluoroboradiaza-*S*-indacence	KH_2PO_4–Na_2HPO_4 buffer	0.08–4.0 μmol L^{-1}	10 nmol L^{-1}	19
1,2-diaminoanthraquinone	poly 2-hydroxyethyl methacrylate	Not reported	10^{-4} mol L^{-1}	20
Pyrene butyric acid (PBA) and Tris(2,2'-bipyridine)ruthenium(II) ($[Ru(bpy)_3]^{2+}$)	SDS micelles for PBA or phosphate buffer for $[Ru(bpy)_3]^{2+}$	5×10^{-5} and 7×10^{-3} mol L^{-1}	Not reported	21
Pyrene butyric acid (PBA) and Tris(2,2'-bipyridine)ruthenium(II) ($[Ru(bpy)_3]^{2+}$) and magnesium phthalocyanine (Mg-Pc)	Polymer thin films	5×10^{-7} and 2.1×10^{-4} mol L^{-1}	1.50×10^{-7} 1.54×10^{-6} 7.8×10^{-7} mol L^{-1}	This study

NR: not reported, Ref.: reference

porosity of the membranes.[27] We did not observe any aggregates or clusters due to the presence of ionic liquid. This indicates that the ionic liquid was evenly distributed on the surface. The electrospun membranes provide higher surface area when compared with thin film membranes. Wang et al. reported that the porous structure of the electrospun membranes provides a surface area-to-volume ratio roughly 1 to 2 orders of magnitude higher than that known for continuous thin films.[28] The development of nanofibers with different sizes can be obtained by changing the parameters of the electrospinning process such as the solvent composition, the concentration of the reactants, the viscosity of the polymer cocktail, the temperature and humidity of the electrospinning cabin, and the distance between the metal needle and the casting plate.[29]

2.2. Spectral response of the pyrene dye to TEMPO radical

We evaluated the NO quenching efficiency of the encapsulated pyrene in solid state. The nitroxyl radical of TEMPO was used as a stable form of NO. We constructed optical chemical sensors in the form of thin films and

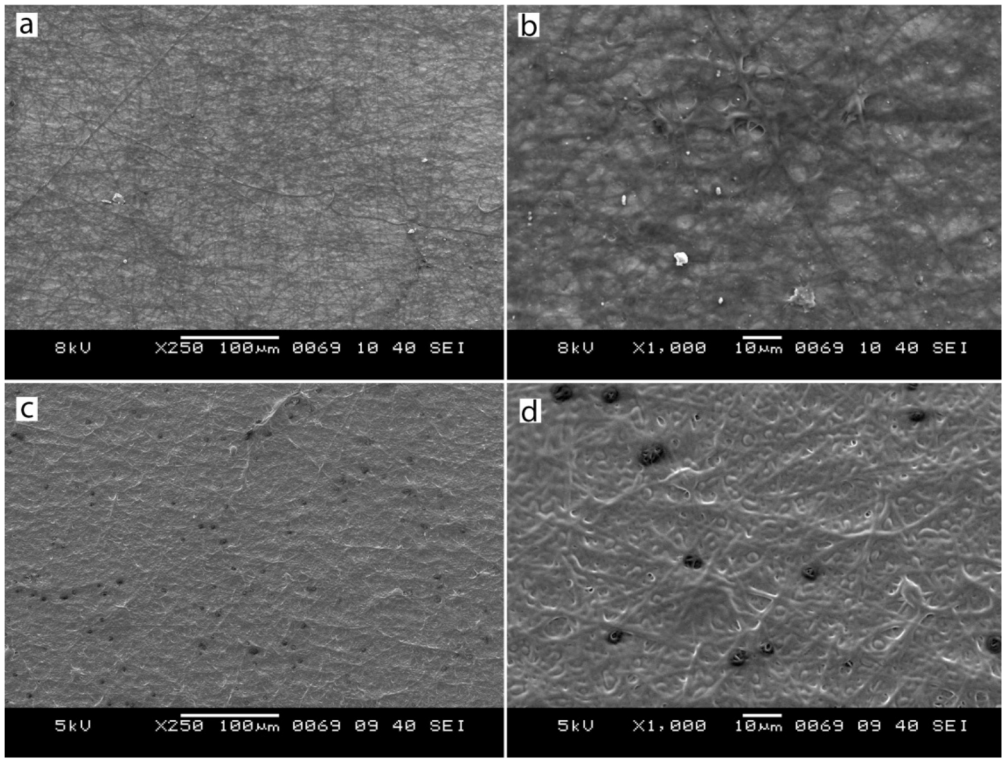

Figure 1. SEM images of IL containing electrospun membranes prepared from P5 and P6 (a: P5, $\times 250$, without AgNPs; b: P5, $\times 1000$; without AgNPs, c: P6, $\times 250$, with AgNPs; and d: P6, $\times 1000$, with AgNPs).

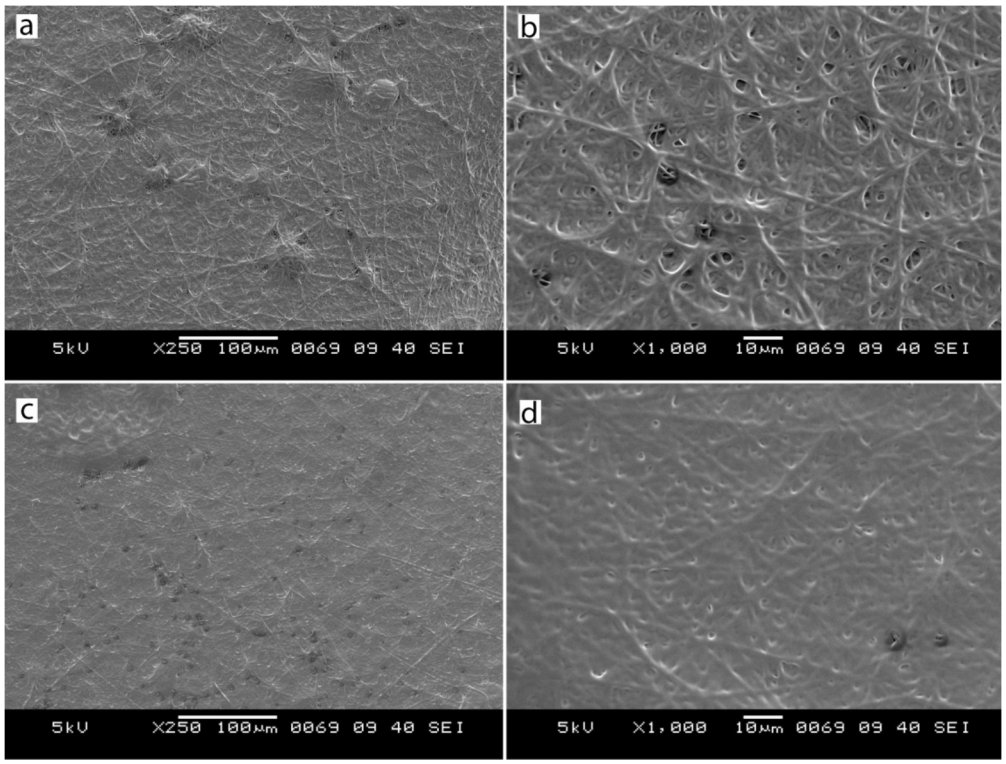

Figure 2. SEM images of electrospun membranes prepared from M4 and M5 (a: M4, $\times 250$, without AgNPs; b: M4, $\times 1000$; without AgNPs, c: M5, $\times 250$, with AgNPs; and d: M5, $\times 1000$, with AgNPs).

electrospun fibers prepared from different cocktail compositions (P1–P9) of plasticized PVC (see Tables 2 and 3). Our previous studies encouraged us to use ionic liquids and silver nanoparticles as additives for the enhancement of the sensor response.[24,25,30] Ozturk et al. utilized silver nanoparticles for oxygen sensing purposes and obtained many advantages such as linear calibration plot, tuned sensitivity, and wide concentration range.[24] Kacmaz et al. manipulated the pH induced sensitivity of the sensing agent by utilizing silver nanoparticles.[25] Oter et al. designed a gaseous CO_2 sensor by exploiting ionic liquids that enhanced the long-term stability of their sensor.[30] We also tested the sensing agents in three different moieties: ultrapure water, phosphate buffer at pH 7.4, and SDS micelles. The tested moieties were all aqueous solutions as the determination of nitric oxide is especially significant in aqueous biological environments as it is the key biochemical messenger and signaling molecule in cells. It also has an important role in immune and blood pressure regulation systems. pH 7.4 is selected as the pH of blood and tissue fluids and the SDS micelles mimic the cell environment. In all of the test moieties the pyrene dye exhibited excitation and emission maxima around 340 and 390 nm, respectively. Presence of the AgNPs did not have a significant effect on the spectral properties. The average Stoke's shift was 50 nm. By the addition of increasing amounts of NO radical onto the PVC encapsulated pyrene, the emission peak at 390 nm exhibited a quenching-based decrease. It is known that the pyrene dye exhibits a quenching-based response to nitric oxide. The quenching was evaluated for the solution phase many times. The quenching is paramagnetic and takes place with TEMPO lower than millimolar concentrations. The simplest method for modeling the quenching phenomena is to use the Stern–Volmer equation (1, 2):[21]

Table 2. Cocktail compositions for PVC-based thin films and electrospun fibers.

Cocktail name	Thin film/ Electrospun	Matrix (PVC)	Plasticizer (DOP)	Dye solution (2.47×10^{-3} M)	Ionic liquid [$BMIM^+$] [PF_6^-]	Nanosilver	Solvent (THF)
P1, P3	TF	120 mg	240 mg	Pyrene 50 μL	-	-	1.5 mL
P2, P4, P7	TF	120 mg	240 mg	Pyrene 50 μL	36 mg	-	1.5 mL
P5, P8	ESF	120 mg	240 mg	Pyrene 50 μL	36 mg	-	1.5 mL
P6, P9	ESF	120 mg	240 mg	Pyrene 50 μL	36 mg	2 mg	1.5 mL
R1	TF	120 mg	240 mg	$Ru(bipy)_3^{2+}$ 50 μL	36 mg	-	1.5 mL
R2	ESF	120 mg	240 mg	$Ru(bipy)_3^{2+}$ 50 μL	36 mg	-	1.5 mL
M1	TF	120 mg	240 mg	Mg-Pc 50 μL	-	-	1.5 mL
M2	TF	120 mg	240 mg	Mg-Pc 50 μL	36 mg	-	1.5 mL
M3	TF	120 mg	240 mg	Mg-Pc 50 μL	36 mg	2 mg	1.5 mL
M4	ESF	120 mg	240 mg	Mg-Pc 50 μL	36 mg	-	1.5 mL
M5	ESF	120 mg	240 mg	Mg-Pc 50 μL	36 mg	2 mg	1.5 mL

TF: Thin film

ESF: Electrospun fiber

$$\frac{I_0}{I} = \frac{\tau_0}{\tau} = 1 + K_{SV}[Q] \quad (1)$$

$$K_{SV} = \tau_0 k_q, \quad (2)$$

where I and I_0 are the fluorescence intensities in the presence and absence of quencher. K_{SV} is the Stern–Volmer constant and [Q] is the quencher concentration. The plot of I_0/I versus [Q] yields a straight line with

Table 3. The Stern–Volmer plots, regression coefficients, and Stern-Volmer constants of all of the studied composites for pyrene dye.

Cocktail name	Medium	Stern–Volmer plots	$K_{sv}[TEMPO]^-$ (μM^{-1})	Regression coefficient, R^2
P1	Pure water	y = 0.0011x + 1.0344	1.1×10^{-3}	0.9666
P2	Pure water	y = 0.0034x + 1.0231	3.4×10^{-3}	0.9933
P3	Buffer	y = 0.0012x + 1.0141	1.2×10^{-3}	0.9936
P4	Buffer	y = 0.0302x + 0.9764	3.0×10^{-2}	0.9935
P5	Buffer	y = 0.0025x + 1.0235	2.5×10^{-3}	0.9925
P6	Buffer	y = 0.0031x + 0.9963	3.1×10^{-3}	0.9648
P7	SDS	y = 0.0126x + 0.9904	1.26×10^{-2}	0.9903
P8	SDS	y = 0.0075x + 0.8998	7.5×10^{-3}	0.9848
P9	SDS	y = 0.0042x + 0.9459	4.2×10^{-3}	0.9825

a slope K_{SV}. The type of quenching can be assumed as static or dynamic by using this equation. The Stern–Volmer plot can be plotted by using the fluorophore lifetimes (τ_0/τ ratios) when lifetime-based measurements are performed. In the presence of quenchers, the fluorescence intensity should decrease alone if the type of quenching is static, which involves the ground state. In the case of dynamic quenching, both the excited state lifetimes and fluorescence intensities will decrease. Thus, K_{SV} should be the product of τ_0 and k_q, which is the bimolecular quenching rate constant. The k_q value is related to the diffusion controlled limit through quenching efficiency. In all cases, the Stern–Volmer plots presented linear behavior, indicating dynamic quenching for pyrene.

Table 3 reveals Stern–Volmer plots and Ksv constants for the PVC embedded pyrene in different sensing media. The thin film and electrospun fiber forms of the sensing agents exhibited different responses towards the NO. The cocktails of P1 and P3, which did not contain any ionic liquid, exhibited a relative signal change about 20% for the analyte. By the addition of ionic liquid, significant enhancements in buffer and micelle moieties were observed, corresponding to 2.5–4.5-fold enhancements in sensor response (80%–90%). Therefore in further studies we utilized the ionic liquid in all of the matrices as additive. The presence of AgNPs did not cause any hysteresis in the emission spectra and relative signal changes of pyrene. The best response was obtained for the sensor studies with P4. Figure 3 reveals the spectral response of P4, the PVC embedded pyrene dye for thin film forms towards TEMPO in buffered solutions. The slope allows calculating a Stern–Volmer constant of 3.0 $\times$ $10^{-2}\mu M^{-1}$ for the pyrene. This value is higher than the Stern–Volmer constant observed for NO in EtOH solutions, which is given as 0.6 mM^{-1}.[21] This means nearly 50 times enhancement in the K_{SV} value for solid phase studies in the presence of IL. The relative signal change of 80% was attained for the concentration range of 0.0–212.5 μM TEMPO (see Figure 3). By this way the limit of detection (LOD) and limit of quantification (LOQ) values of 0.15 and 0.5 μM were attained. In contrast to our expectations, the electrospun fibers made up of the same material exhibited lower Ksv values with respect to the thin films.

2.3. Spectral response of the $Ru(bipy)_3^{2+}$ for the TEMPO radical

We evaluated the NO quenching of $Ru(bipy)_3^{2+}$ encapsulated in sol-gel slides prepared from different cocktail compositions of R3 and R4 (see Table 4). We tested the sensing response in phosphate buffer at pH 7.4 and in

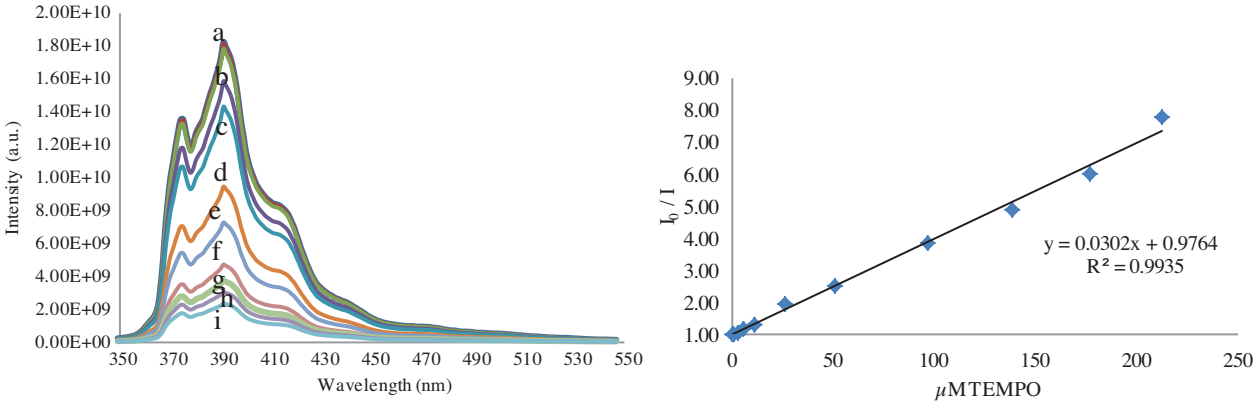

Figure 3. Fluorescence response of pyrene embedded PVC-based thin film (P4) with additive of $[BMIM^+][PF_6^-]$ to TEMPO in pH 7.4 buffer media. (a) 0.0, 0.5 μM, (b) 5.3 μM, (c) 10.5 μM, (d) 25.9 μM, (e) 50.6 μM, (f) 96.6 μM, (g) 138.6 μM, (h) 177.1 μM, (i) 212.5 μM TEMPO.

SDS micelles. In all of the test moieties the $Ru(bipy)_3^{2+}$ dye exhibited excitation and emission maxima around 480 and 610 nm, respectively. The average Stoke's shift was 135 nm. By the addition of increasing amounts of NO radical onto the sol-gel encapsulated $Ru(bipy)_3^{2+}$, the emission peak at 610 nm exhibited a quenching-based decrease. Quenching-based response is explained in section 2.2 in detail. The Stern–Volmer equations were used for the modeling of the quenching phenomena (see Table 5). In all cases, the Stern–Volmer plots presented a linear behavior, indicating the dynamic quenching mechanism for $Ru(bipy)_3^{2+}$. Figure 4 reveals the spectral response of the sol-gel embedded $Ru(bipy)_3^{2+}$ dye with ionic liquid to TEMPO in SDS solutions. As a result, the cocktail of R3, which did not contain any ionic liquid, exhibited a relative signal change of about 7%. By the addition of ionic liquid, significant enhancements in micelle moieties were observed corresponding to 5-fold enhancement in sensor response (37%). Therefore in further studies we utilized the ionic liquid in all of the matrices as additive. The slope allows calculating a Stern–Volmer constant of $2.6 \times 10^{-3} \mu M^{-1}$ for sol-gel encapsulated $Ru(bipy)_3^{2+}$ in SDS solutions. This value is higher than the Stern–Volmer constant observed in NO sensing in the solution phase, which is given as 0.04 mM^{-1} in aqueous solutions.[21] This means nearly 70 times enhancement in the K_{SV} value for solid phase studies.

Table 4. Cocktail compositions for sol-gel slides.

Cocktail name	Dye solution	TEOS (mL)	EtOH (mL)	Acidified water (μL)	Triton- X 100 (μL)	Ionic liquid (μL)	Gelation time (min)	Cocktail pH
R3	$Ru(bipy)_3^{2+}$	1.07	1.07	193*	120	-	120	4.5
R4	$Ru(bipy)_3^{2+}$	1.07	1.07	193*	120	120	120	4.5

2.4. Spectral response of the Mg-phthalocyanine for the TEMPO radical

Mg-Pc dye was excited at 668 nm in all of the test moieties. In all cases the emission maxima appeared at 674–676 nm. The Stoke's shift values were relatively low when compared with pyrene and ruthenium dye and were in the range of 6–8 nm, which is convenient for the Pcs. Figure 5 reveals the spectral response of the PVC

Table 5. The Stern–Volmer plots, regression coefficients, and Stern–Volmer constants of all of the studied composites for $Ru(bipy)_3^{2+}$ dye.

Cocktail Name	Matrix	RTIL	Medium	Stern–Volmer plots	K_{sv} (μM^{-1})	Regression coefficient, R^2
R3	Sol-gel, thin film	–	SDS	y = 0.002x + 1.0694	0.0020	0.9078
R4	Sol-gel, thin film	+	SDS	y = 0.0027x + 1.04337	0.0027	0.9830

Table 6. Equations and regression coefficients of the calibration plots for different cocktail formulations in different sensing media for Mg-Pc dye.

Cocktail name	Thin Film/electro spun fiber	RTIL	Nanos ilver	Medium	Equations of the calibration plots	Regression coefficient
M1	TF	+	–	Buffer	y = 0.0045x + 1.0495	0.9941
M2	TF	+	–	SDS	y = 0.0035x + 1.0250	0.9978
M3	TF	+	+	SDS	y = 0.0042x + 1.0261	0.9949
M4	ESF	+	–	SDS	y = 0.0061x + 1.0142	0.9987
M5	ESF	+	+	SDS	y = 0.0032x + 1.0346	0.9930

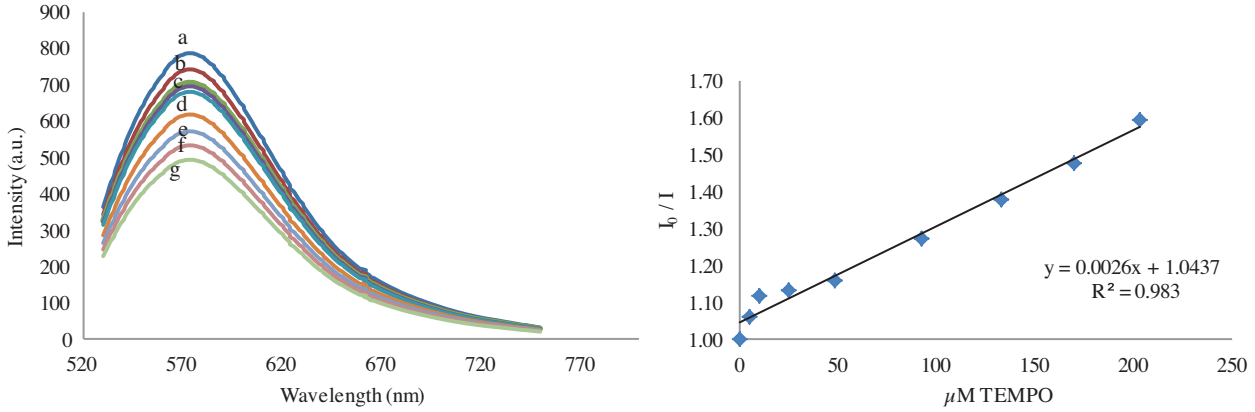

Figure 4. Fluorescence response of $Ru(bipy)_3^{2+}$ in sol-gel fiber (R5) with $[BMIM^+][PF_6^-]$ to TEMPO in pH 7.4 SDS media. (a) 0.0 μM, (b) 5.1 μM, (c) 10.1, 24.8, 48.5 μM, (d) 92.5 μM (e) 132.7 μM (f) 169.6 μM, (g) 203.5 μM TEMPO.

embedded Mg-Pc dye for TEMPO in SDS micelles. Upon exposure to increasing concentrations of TEMPO, the dye exhibited increasing response in signal intensity in a different manner from the response of the pyrene and $Ru(bipy)_3^{2+}$ dyes. This indicates that the response is not quenching-based but a complex formation occurs between the dye and NO. The possible sensing mechanism is given in the Scheme. Silva et al. reported that the highest value of the Fukui function is associated with the most reactive site of the molecule. The Fukui function was the highest for nitric oxide and was found in nitrogen, which means that this site governs a radical interaction.[31]

Nguyen et al. also investigated the mechanism for NO and metal-phthalocyanine interaction.[32] Their numerical calculations showed that NO was strongly chemisorbed to the metal atom and the N terminal of NO prefers to bind with metal atoms rather than with the O terminal. This resulted in a change in the geometric

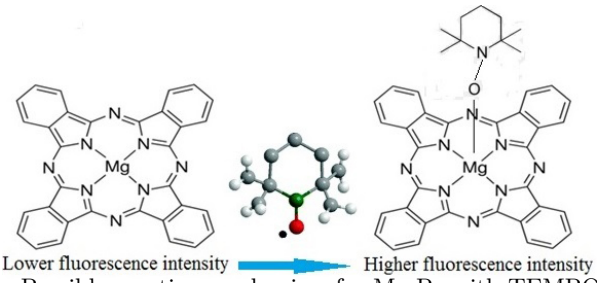

Scheme. Possible reaction mechanism for Mg-Pc with TEMPO radical.

and electronic structure and properties of metal-Pc. They also showed that NO weakly adsorbs on all other nonmetal sites. In their experimental work, they found that electron charge transfer from MPc to NO occurs, which shows that the NO gases absorbed on metal-Pc turn out to be negatively charged and thus form acceptor states since they attract electrons from metal-Pc. As a result, a charge transfer complex was formed with new electrochemical and photochemical properties, enabling the design of new NO sensors.[32] In our case, we applied TEMPO to mimic NO as TEMPO is a stable radical that covalently binds to organic/bioorganic molecules. TEMPO will probably bind at the most reactive site of the molecule, which is the radicalic oxygen site, to form MgPcTEMPO complex with a 4 + 1 coordination of Mg. Kinzhybalo et al. reported that generally 4 + 1 coordination of Mg in MgPcL complexes is observed in the case of O-donor ligands and 4 + 2 coordination of Mg for N-donor ligands.[33] Moreover, sterical hindrances on the nitrogen site of TEMPO will forward the binding from the oxygen terminal. The Mg center can also undergo a possible reduction or oxidation in the presence of TEMPO with new photochemical properties. Vilakazi et al. found that the complex formation of Co-Pc with NO was accompanied by electron transfer from the central Co (II) metal to the NO.[34]

Table 6 reveals equations of the calibration plots and the sensor performances for different cocktail formulations of different sensing media in a cooperative manner. As a result, electrospun fiber forms of the dye exhibited the highest relative signal change towards TEMPO when tested in micelle solutions. When the thin films were changed with the electrospun membranes the relative signal change enhanced from 40% to 68% for the electrospun membranes. The LOD and LOQ values were 0.78 and 2.6 μM, respectively. The calibration plots exhibited good slopes and linearity (see Table 6 and inset of Figure 5). Regression coefficients of 0.9930–0.9987 can be concluded as the indicator of the desired linearity. Presence of the AgNPs within the matrix did not result in a significant change in signal response in terms of linearity and sensitivity but only facilitated the production of electrospun fibers.

2.5. Lifetime-based measurements

TEMPO was frequently studied in solution phase as a paramagnetic fluorescence quencher, with $[Ru(bpy)_3]^{2+}$ as well as pyrene. The excited molecule is deactivated in a nonradiative manner to its ground state due to collisions with the oxygen, which is called dynamic quenching. In dynamic quenching, the increase in nitric oxide concentration results in a decrease both in the fluorescence intensity and lifetime of the $[Ru(bpy)_3]^{2+}$ and pyrene dyes. The fluorescence lifetimes were recorded in all of the test moieties in the absence and presence of ionic liquid and silver nanoparticles. The pyrene dye was excited with a laser light source at 357 nm (laser with 890 ps pulse width). In all of the examined moieties, the pyrene dye exhibited multiexponential decay in contrast to aqueous solutions, which can be attributed to the presence of heterogeneous sites in the polymeric matrix. The decay responses and the corresponding calibration plot for the tested media are shown in Figures 6 and

7 and Figure 8, respectively. Table 7 shows the decay times, chi-square values, diffusion controlled quenching rate constants (kq), and lifetime-based Stern–Volmer constants of the studied composites in the presence and in absence of TEMPO. These lifetimes ranged from 85 to 145 ns for the long lifetime component and 1.9 to 13.7 ns for the short one. The contribution of the longer lifetime component to mean lifetime was dominant and at an average of 90.0% in both the absence and presence of quencher. In the presence of TEMPO, the long lifetime component exhibited a slight decrease for the P3–P9. The presence of ionic liquid enhanced the lifetime value and the sensing response of the pyrene dye, while nanosilver particles decreased the lifetime especially in SDS media. Thus, the best relative signal change and the highest kq value were obtained in buffer solution for thin film forms containing ionic liquid. This result is in accordance with the data obtained from steady state measurements. The Stern–Volmer constants of pyrene dye obtained from steady state measurements are higher than those obtained from lifetime measurements; thus fluorescence intensity-based response is more advantageous for the design of new optical NO sensors.

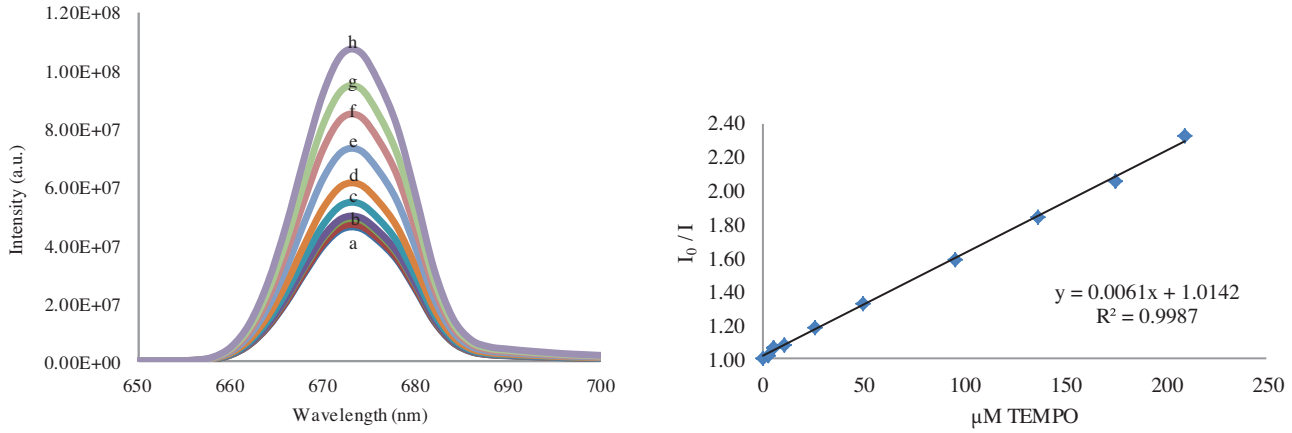

Figure 5. Fluorescence response of Mg-Pc embedded PVC-based electrospun fiber (M4) with additive of $[BMIM^+][PF_6^-]$ to TEMPO in pH 7.4 SDS media. (a) 0.0, 2.6 μM, (b) 5.1, 10.4 μM, (c) 25.6 μM, (d) 49.9 μM, (e) 95.4 μM, (f) 136.9 μM, (g) 174.9 μM, (h) 209.9 μM TEMPO.

The $Ru(bipy)_3^{2+}$ dye was excited with a laser light source at 467 nm (laser with 118.2 ps pulse width) and the decay characteristics were measured in TEMPO-free TEMPO containing moieties at emission wavelength of 610 nm. $Ru(bipy)_3^{2+}$ dye is known for its lifetime value near 600 ns in solution phase.[14] When embedded in the solid phase the lifetime enhanced to nearly 1500 ns values. For all of the sensing slides, the fluorescence decay was monoexponential and the lifetimes ranged between 1324 and 1537 ns (see Table 7). In the presence of TEMPO, when compared with pyrene dye, $Ru(bipy)_3^{2+}$ dye exhibited less relative signal change in the decay time and we did not utilize the lifetimes as a calibration tool. The decrease in lifetime value was 11% and 10% for thin film and electrospun slides, respectively.

The fluorescence lifetimes were also recorded for PVC embedded forms of the Mg-Pc dye. The dye was excited at 668 nm with the microsecond flash lamp of the FLS 920 and the lifetimes were recorded at the emission wavelength of 674 nm. The decay characteristics were measured for electrospun fibers and thin films in TEMPO-free, 51.6 and 206.4 μM TEMPO-containing buffer solutions, and/or SDS solutions. The data reveal that, when compared with thin films, the decay time of electrospun fibers was enhanced from 1416 μs to 2739 μs. By the addition of TEMPO, increasing lifetime values were observed for magnesium dye, different from the quenching-based response of pyrene and ruthenium dyes (see Table 7). This was an expected result

Table 7. Summary of the decay characteristics and chi square values of the studied composites in presence and absence of TEMPO

Cocktail name	τ_0 (ns)	τ_0, average	χ^2	τ_{TEMPO} (ns)	τ_{TEMPO} average	χ^2	K_{sv} (μM^{-1})	k_q (μM^{-1} s^{-1})
P3	4.52 ± 0.18 (5.8%)	118.86	1.099	4.24 ± 0.17 (6.3%)	109.93	1.072	1.2×10^{-3}	1.0×10^{-5}
	125.90 ± 11.39 (94.2%)			117.04 ± 10.31 (93.7%)				
P4	4.28 ± 0.18 (4.8%)	138.38	1.064	4.28 ± 0.18 (6.3%)	106.26	1.123	3.0×10^{-2}	2.2×10^{-4}
	145.14 ± 15.85 (95.2%)			113.12 ± 9.42 (93.7%)				
P5	4.46 ± 0.19 (6.1%)	120.29	1.156	4.28 ± 0.17 (6.9%)	105.85	1.031	2.5×10^{-3}	2.1×10^{-5}
	127.81 ± 13.70 (93.9%)			113.38 ± 9.96 (93.1%)				
P6	4.65 ± 0.25 (6.7%)	107.35	1.026	4.02 ± 0.23 (6.1%)	101.07	1.078	3.1×10^{-3}	2.9×10^{-5}
	114.72 ± 13.22 (93.3%)			107.37 ± 10.97 (93.9%)				
P7	1.88 ± 0.03 (8.6%)	79.82	1.186	1.82 ± 0.03 (9%)	74.54	1.174	1.26×10^{-2}	1.6×10^{-4}
	87.15 ± 2.32 (91.4%)			81.73 ± 2.00 (91%)				
P8	1.98 ± 0.04 (8%)	79.40	1.104	1.70 ± 0.02 (11.7%)	71.89	1.160	7.5×10^{-3}	9.5×10^{-5}
	85.74 ± 2.38 (92%)			81.19 ± 1.97 (88.3%)				
P9	13.70 ± 0.26 (66%)	38.57	1.088	12.34 ± 0.23 (66%)	32.40	1.174	4.2×10^{-3}	1.1×10^{-4}
	86.86 ± 5.8 (34%)			71.34 ± 3.80 (34%)				
R1	1537.89 ± 9.85 (100%)	1537.89	1.199	1371.21 ± 9.07 (100%)	1371.21	1.385	2.7×10^{-3}	1.8×10^{-6}
R2	1467.84 ± 13.54 (100%)	1467.84	1.223	1324.84 ± 11.24 (100%)	1324.84	1.200	1.3×10^{-3}	8.9×10^{-7}
M1	1416.31 ± 37.08	1416.31	1.200	2018.39 ± 63.25 (100%)	2018.34	1.225	-	-
M2	241.73 ± 4.95 (24.7%)	1660.37	1.189	294.60 ± 5.68 (23.1%)	1885.63	1.142	-	-
	2125.71 ± 35.71 (75.3%)			2363.56 ± 37.34 (76.9%)				
M4	2720.94 ± 8.94 (100%)	2720.94	1.155	2739.04 ± 10.06 (100%)	2739.04	1.138	-	-

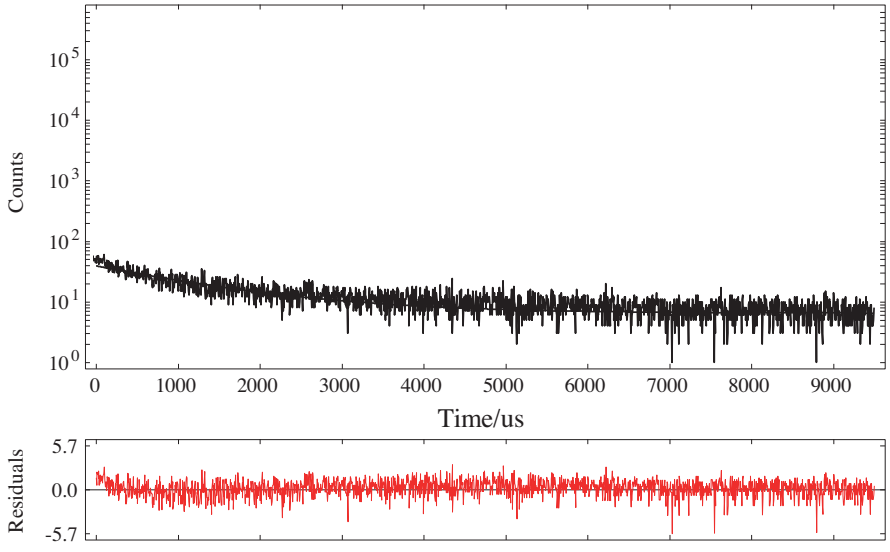

	Fix	Value / µs	Std. Dev / µs		Fix	Value	Std. Dev	Rel %
τ_1	☐	1416.3130	37.08256	B_1	☐	32.673	0.6539	100.00
τ_2	☐			B_2	☐			
τ_3	☐			B_3	☐			
τ_4	☐			B_4	☐			
				A	☐	6.471		

χ^2 : 1.200

Figure 6. Decay response of Mg-Pc embedded PVC-based thin film (M1) with additive of $[BMIM^+][PF_6^-]$ in pH 7.4 buffer media without TEMPO solution.

as the Mg-phthalocyanine response in steady state measurements was also increasing due to complex formation between the dye and the TEMPO radical. The fluorescence decay was monoexponential in buffer media while it was multiexponential in SDS media. Multiexponential decays are expected for heterogeneous media such as micelle solutions like SDS.[21] The first lifetime was nearly at 250 μs levels, while the second was nearly at 2200 μs levels. The contribution of the longer lifetime component to mean lifetime was dominant and at an average of 75%. For buffered solutions, the decay time was monoexponential and the best response was observed for thin film forms, which exhibited a 42% increase in the lifetime value from 1437 μs to 2017 μs when 206.4 μM concentration of TEMPO was added.

3. Experimental

3.1. Materials

Nitric oxide sensitive fluorescent dyes, pyrene, magnesium phthalocyanine (Mg-Pc), and tris(2,2'-bipyrdyl)dichlororuthenium(II) hexahydrate ($Ru(bipy)_3^{2+}$) were supplied by Aldrich. Polyvinylchloride (PVC, high molecular weight) and dioctyl phthalate (DOP, plasticizer) were obtained from Aldrich. Silver nitrate (99% $AgNO_3$) and sodium borohydride (99% $NaBH_4$) were from Merck and Aldrich, respectively. The ionic liquid (RTIL),

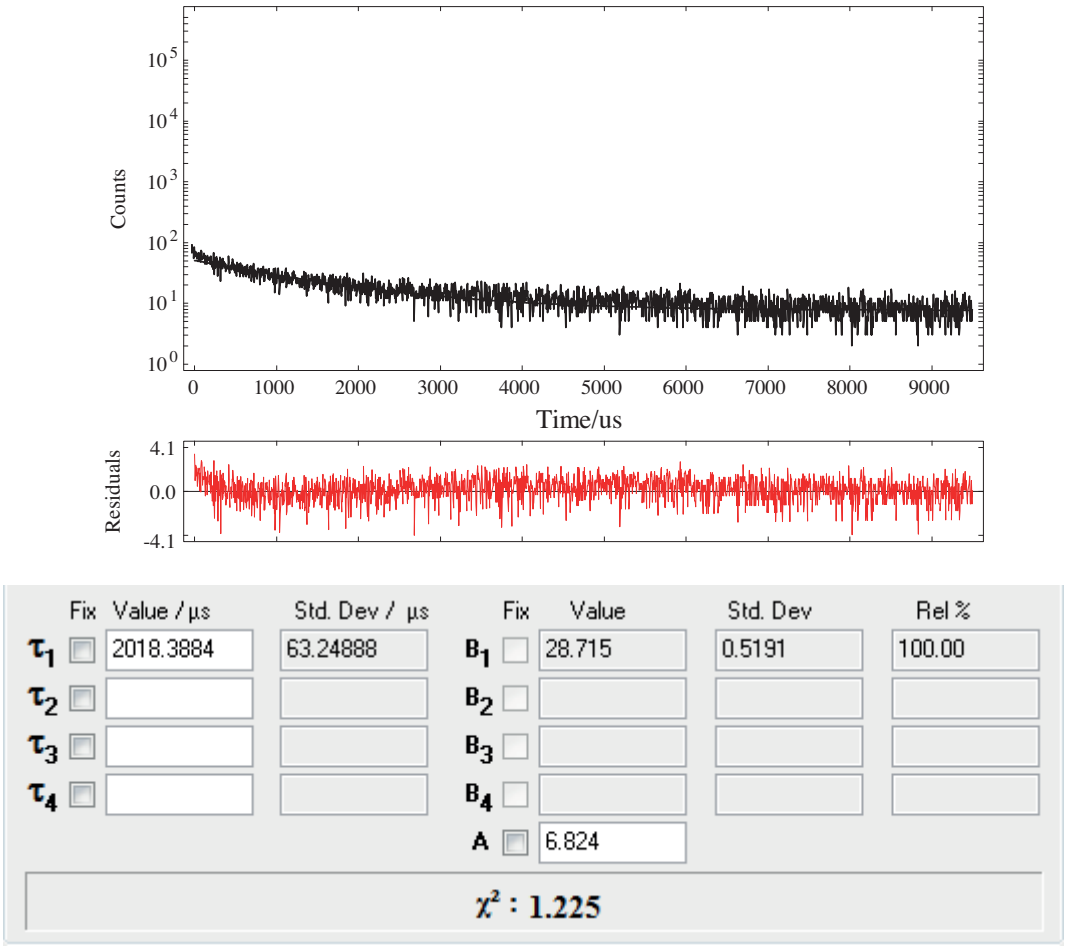

Figure 7. Decay response of Mg-Pc embedded PVC-based thin film (M1) with additive of $BMIM^+][PF_6^-]$ in the presence of 206.4 μM TEMPO in pH 7.4 buffer media.

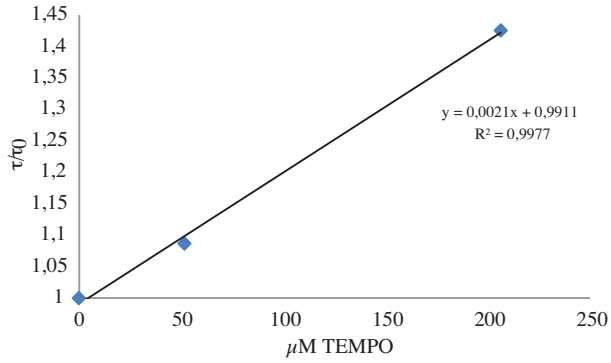

Figure 8. Variation in the lifetime ratio (τ / τ_0) versus μM TEMPO concentrations in pH 7.4 buffer.

1-butyl-3-methylimidazolium hexafluorophosphate, $[BMIM^+][PF_6^-]$, was from Merck. The nitric oxide radical was the free and stable radical of TEMPO (98%, 2,2,6,6-tetramethyl-1-biperidinyloxy) from Aldrich. Sodium dodecyl sulfate (SDS) was from Merck and used as anionic surfactant. Analytical grade solvents and Millipore ultrapure water were used.

3.2. Preparation of the solutions

The sensing studies were conducted in three different environments: in unbuffered aqueous solutions, in pH 7.4 (intracellular pH) buffered aqueous solutions, and in pH 7.4 buffered SDS solutions, which imitate the biological cell environment. The stock TEMPO solution was prepared with deoxygenated ethanol (EtOH) as it is not stable under oxygenated conditions. The standard solutions were prepared freshly prior to the experiments. The buffer solutions of pH 7.4 were prepared using $NaH_2PO_4.2H_2O$ and $Na_2HPO_4.12H_2O$ in ultrapure water. The solution pH was adjusted using either 0.1 M HNO_3 or 0.1 M NaOH. The SDS solution was prepared as 0.01 M in 0.4 M NaCl containing pH 7.4 phosphate buffer and then sonicated for 15 min.

3.3. Apparatus

The steady state florescence measurements were recorded with a Varian Cary Eclipse and an Edinburgh Instruments spectrometer. Fluorescence lifetime measurements were performed by single photon counting technique (TCSPC) with an FLS920 (Edinburgh Instruments). The excitation was performed for pyrene and $Ru(bipy)_3^{2+}$ dyes with the 367.8 nm pulsed laser source with a pulse width of 790.4 ps. The emission data were collected at 390 nm and 610 nm for the two dyes, respectively. A microsecond flash lamp was utilized for the excitation of the phthalocyanine dye. The lifetime data were recorded after deconvolution with a weighted, nonlinear least-squares method. The obtained chi-square values were less than 1.2 and the residuals were symmetrically distributed around the zero axes. A programmable syringe pump (Top-5300) and Gamma High Voltage ES30 (high voltage power supply) were utilized for the fabrication process of electrospun fibers. The surface structure of the sensor slides was examined using a 6060-JEOL JSM scanning electron microscope.

3.4. Fabrication of silver nanoparticles

Silver nanoparticles were produced according to the literature method.[22,35] Briefly, in this method, 1.0 mM silver nitrate (10 mL volume) was added dropwise into 2.0 mM sodium borohydride (30-mL volume) in an ice bath while stirring continuously. The color of the resulting colloidal solution was pale yellow at the beginning. The following colors were purple and finally gray. The sodium borohydride solution was used to reduce the ionic silver and to keep the silver nanoparticles apart from each other in a coordinated form with the anions of BH_4^-. The centrifuge (6000 RPM) method was used to separate the silver nanoparticles dispersed in water. The size distribution analysis and other data regarding the characterization of silver nanoparticles were given previously.[36,37]

3.5. Fabrication of thin films, sol-gel films, and electrospun slides

The sensing composites were prepared in glass vials to contain 33% PVC and 66% DOP. The cocktails were mixed by a magnetic stirrer for a while after addition of the solvent, THF. The homogeneous cocktail was spread on polyester support (Mylar Du Pont) and the thin films were left in a desiccator saturated with the solvent vapor for drying. The Mylar support was optically transparent and ion impermeable. It also exhibited good adhesion to the PVC membrane. The compositions of the cocktails are given in Table 2.

In order to obtain electrospun slides, the homogeneous PVC cocktails were placed in a 10-mL plastic syringe. The syringe was fixed on the syringe pump and the electrode of the power supply was clamped to the metal needle of the syringe. The feed rate and the voltage were adjusted to 2.0 mL/h and 25–30 kV, respectively. The electrospun fibers were collected on an aluminum foil-coated substrate (see Table 2).

The sol-gel matrix was utilized for the sensor studies of $Ru(bipy)_3^{2+}$ dye due to the leaching effects in PVC matrices. The sol-gel slides were prepared from a solution containing tetraethyl orthosilicate (TEOS), HCl, water, ethanol, ethanolic solution of the dye, Triton X-100, and ionic liquid. For comparison, ionic liquid-free cocktails were also prepared. The preparation procedure of the sol-gel cocktails was explained before in detail.[38] Finally, optically transparent crack-free thin films were prepared. The concentration of $Ru(bipy)_3^{2+}$ dye was 10^{-3} M in the sol. The exact compositions of the sols are given in Table 4.

4. Conclusions

In this work we utilized pyrene, $Ru(bipy)_3^{2+}$, and Mg-Pc dyes as NO sensitive molecular probes in embedded form for the first time. We fabricated thin films and electrospun fibers to prepare the sensing agents. Pyrene and Mg-Pc were doped in plasticized PVC along with ionic liquid and AgNPs, whereas the $Ru(bipy)_3^{2+}$ dye was encapsulated in TEOS-based sol-gel. The response was evaluated by both steady state and lifetime-based measurements. Both the pyrene and the $Ru(bipy)_3^{2+}$ dyes exhibited emission-based response towards the NO radical in direction of decrease in signal intensity. The best spectral response to TEMPO was attained for the PVC-embedded pyrene in the presence of ionic liquid along with AgNPs with steady state measurements. The relative signal change of 80% was observed for the concentration range of 0.0–212.5 μM of the TEMPO. LOD and LOQ values were 0.15 μM and 0.5 μM, respectively. Similar studies were performed for the $Ru(bipy)_3^{2+}$ dye. The relative signal change of 50% was attained for the concentration range of 0.0–207.4 μM of nitric oxide. LOD and LOQ values were 1.54 μM and 5.1 μM, respectively. Spectral response of the PVC-embedded Mg-Pc dye to TEMPO in buffered solutions and in SDS micelles was also recorded. Different from the other dyes, the Mg-Pc dye exhibited increasing fluorescence intensity and lifetime-based response to NO. Lifetime-based response is more advantageous and selective especially in biological samples as they are not affected by source variations, photo-bleaching, or leaching of the probe materials or changes in the efficiency of the optical systems. Another advantage of the Mg-Pc dye is that it is not poisonous for organic systems. In both of the moieties the emission-based response appeared at 674 nm and upon exposure to the increasing concentrations of the TEMPO the signal intensity increased. The relative signal change of 68% was attained for the concentration range of 0.0–220.1 μM TEMPO. The LOD and LOQ values of 0.78 and 2.6 μM were extracted from the calibration plots.

Acknowledgments

Funding for this research was provided by the Scientific Research Funds of Dokuz Eylül University 2012.KB.FEN.049. We also thank the Scientific and Technological Research Council of Turkey (TÜBİTAK) and TÜBİTAK-BİDEB.

References

1. McVeigh, G. E.; Hamilton, P.; Wilson, M.; Hanratty, C. G.; Leahey, W. J.; Devine, A. B.; Morgan, D. G.; Dixon, L. J.; McGrath, L. T. *Circulation* **2002**, *106*, 208-213.
2. Merrill, J. E.; Murphy, S. P.; Mitrovic, B.; Mackenzie-Graham, A.; Dopp, J. C.; Ding, M. Z.; Griscavage, J.; Ignarro, L. J.; Lowenstein, C. J. *J. Neurosci. Res.* **1997**, *48*, 372-384.
3. Moncada, S.; Bolanos, J. P. *J. Neurochem.* **2006**, *97*, 1676-1689.
4. Ciszewski, A.; Milczarek, G. *Talanta* **2003**, *61*, 11-26.
5. Diab, N.; Schuhmann, W. *Electrochim. Acta* **2001**, *47*, 265-273.
6. Silva, J. F.; Griveau, S.; Richard, C.; Zagal, J. H.; Bedioui, F. *Electrochem. Commun.* **2007**, *9*, 1629-1634.

7. Ishimura, Y.; Gao, Y. T.; Panda, S. P.; Roman, L. J.; Masters, B. S.; Weintraub, S. T. *Biochem. Biophys. Res. Commun.* **2005**, *338*, 543-549.
8. Funazo, K.; Tanaka, M.; Shono, T. *Anal. Chim. Acta* **1980**, *119*, 291-297.
9. Kleschyov, A. L.; Wenzel, P.; Munzel, T. *J. Chromatogr. B* **2007**, *851*, 12-20.
10. Hall, D. M.; Buettner, G. R.; Gisolfi, C. V. *Microchem. J.* **1997**, *56*, 165-170.
11. Yang, L. H.; Ahn, D. J.; Koo, E. *Int. J. Nanomed.* **2014**, *10*, 115-123.
12. Itoh, Y.; Ma, F. H.; Hoshi, H.; Oka, M.; Noda, K.; Ukai, Y.; Kojima, H.; Nagano, T.; Toda, N. *Anal. Biochem.* **2000**, *287*, 203-209.
13. Hu, X.; Zhang, X.; Song, H.; He, C.; Bao, Y; Tang, Q.; Duan, C. *Tetrahedron* **2012**, *68*, 8371-8375.
14. Kumar, P.; Kalita, A.; Mondal, B. *Inorg. Chim. Acta* **2013**, *404*, 88-96.
15. Dacres, H.; Narayanaswamy, R. *Sensors Actuators B* **2004**, *107*, 14-23.
16. Ding, L.; Fan, C.; Zhong, Y.; Li, T.; Huang, J. *Sensors Actuators B* **2013**, *185*, 70-76.
17. Esquembre, R.; Pastor, I.; Mallavia, R.; Mateo, C. R. *J. Photochem. Photobiol. A: Chem.* **2005**, *173*, 384-389.
18. Yu, M.; Wang, W.; Zhang, N. *Spectrochim. Acta A: Mol. Biomol. Spectrosc.* **2014**, *126*, 329-332.
19. Zhang, X.; Chi, R.; Zou, J.; Zhang, H. S. *Spectrochim. Acta A* **2014**, *60*, 3129-3134.
20. 20. Hong, W. Y.; Yang, T. W.; Wang, C. M.; Syu, J. H.; Lin, Y. C.; Meng, H. F.; Tsai, M. J.; Cheng, H.; Zan, H. W.; Horng, S. F. *Org. Electro.* **2013**, *14*, 1136-1141.
21. Oter, O.; Ribou, A. C. *J. Fluoresc.* **2009**, *19*, 389-397.
22. Lan, E. H.; Dave, B. C.; Fukuto, J. M.; Dunn, B.; Zink, J. I.; Valantine, J. S. *J. Mater. Chem.* **1999**, *9*, 45-53.
23. Dacres, H.; Narayanaswamy, R. *Sens. Actuators, B* **2005**, *107*, 14-23.
24. Dacres, H.; Narayanaswamy, R. *Aust. J. Chem.* **2008**, *61*, 189-196.
25. Kacmaz, S.; Ertekin, K.; Oter, O.; Hizliateş, C. G.; Ergun, Y.; Celik, E. *J. Lumin.* **2015**, *168*, 228-235.
26. Wang, K.; Ma, Q.; Wang, S.D.; Liu, H.; Zhang, Z. S.; Bao, W.; Zhang, K. Q.; Ling, L. Z. *Applied Physics A* **2016**, *122*, 40-49.
27. Öter, Ö.; Şahin, G. S. *Turk. J. Chem.* **2015**, *39*, 395-411.
28. Wang, X.; Drew, C.; Lee, S. H.; Senecal, K. J.; Kumar, J.; Samuelson, L. A. *Nano Letters* **2002**, *2*, 1273-1275.
29. Deitzel, J. M.; Kleinmeyer, J.; Tan, N. C. *Polymer* **2001**, *42*, 261-272.
30. Oter, O.; Sabanci, G.; Ertekin, K. *Sensor Letters* **2013**, *11*, 1591-1599.
31. Silva, V. H. C.; Martins, M. P.; Oliveira, H. C. B.; Camargo, A. *Journal of Molecular Graphics and Modelling* **2011**, *29*, 777-783.
32. Nguyen, T. Q.; Escaño, M. C. S.; Kasai, H. *J. Phys. Chem. B* **2010**, *114*, 10017-10021.
33. Kinzhybalo, V.; Kubiak, R.; Janczak, J. *Polyhedron* **2010**, *115*, 142-154.
34. Vilakazi, S.; Nyokong, T. *Polyhedron* **2000**, *19*, 229-234.
35. Solomon, S. D.; Bahadory, M.; Jeyarajasingam, A. V.; Rutkowsky, S. A.; Boritz, C. *J. Chem. Education* **2007**, *84*, 322-325.
36. Ozturk, O.; Oter, O.; Yildirim, S.; Subasi, E.; Ertekin, K.; Celik, E.; Temel, H. *J. Lumin.* **2014**, *155*, 191-197.
37. Ongun, M. Z.; Oter, O.; Sabancı, G.; Ertekin, K.; Celik, E. *Sensors Actuators B* **2013**, *183*, 11-19.
38. Oter, O.; Ertekin, K.; Derinkuyu, S. *Materials Chemistry and Physics* **2001**, *113*, 322-328.